

Magneto-optics of massive Dirac fermions in bulk Bi₂Se₃

M. Orlita,^{1,*} B. A. Piot,¹ G. Martinez,¹ N. K. Sampath Kumar,¹ C. Faugeras,¹
M. Potemski,¹ C. Michel,² E. M. Hankiewicz,² T. Brauner,³ Č. Drašar,⁴ S. Schreyeck,⁵
S. Grauer,⁵ K. Brunner,⁵ C. Gould,⁵ C. Brüne,⁵ and L. W. Molenkamp⁵

¹*Laboratoire National des Champs Magnétiques Intenses,*

CNRS-UJF-UPS-INSA, 25, avenue des Martyrs, 38042 Grenoble, France

²*Institute for Theoretical Physics, TP IV, University of Würzburg, Am Hubland, D-97074 Würzburg, Germany*

³*Institute for Theoretical Physics, Vienna University of Technology, A-1040 Vienna, Austria*

⁴*Faculty of Chemical Technology, University of Pardubice, CZ-53210 Pardubice, Czech Republic*

⁵*Physikalisches Institut (EP III), Universität Würzburg, D-97074 Würzburg, Germany*

(Dated: April 14, 2015)

We report on magneto-optical studies of Bi₂Se₃, a representative member of the 3D topological insulator family. Its electronic states in bulk are shown to be well described by a simple Dirac-type Hamiltonian for massive particles with only two parameters: the fundamental bandgap and the band velocity. In a magnetic field, this model implies a unique property – spin splitting equal to twice the cyclotron energy: $E_s = 2E_c$. This explains the extensive magneto-transport studies concluding a fortuitous degeneracy of the spin and orbital split Landau levels in this material. The $E_s = 2E_c$ match differentiates the massive Dirac electrons in bulk Bi₂Se₃ from those in quantum electrodynamics, for which $E_s = E_c$ always holds.

PACS numbers: 71.70.Di, 76.40.+b, 78.30.-j, 73.20.-r

Inspiring analogies to relativistic systems have largely helped to elucidate the electronic properties of two-dimensional graphene [1, 2], surface states of topological insulators (TIs) [3–6], novel three-dimensional (3D) semimetals [7–9] as well as certain narrow gap semiconductors [10]. Here, we report on magneto-optical studies of bulk Bi₂Se₃, which imply the approximate applicability of the Dirac Hamiltonian for massive relativistic particles to approach the band structure of this popular representative of the TI family.

The dispersion relations of genuine massive Dirac fermions in quantum electrodynamics are defined by two parameters: the energy gap 2Δ between particles and antiparticles and velocity parameter v_D . At low energies, *i.e.*, in the non-relativistic limit, these dispersions become parabolic and characterized by the same effective mass $m_D = \Delta/v_D^2$ (rest Dirac mass). Such dispersions resemble the cartoon sketch of a direct gap semiconductor, which may be conventionally described using Schrödinger equation, completed by extra Pauli terms in order to include the spin degree of freedom. In contrast, no additional terms are needed when Dirac equation is employed, since it inherently accounts for spin-related effects. For instance, when the magnetic field B is applied, Dirac equation describes both cyclotron (E_c) as well as spin (E_s) splitting of the electronic states and implies that these two splitting energies are the same and linear with B in the non-relativistic approximation: $E_s = E_c = \hbar\omega_c = \hbar eB/m_D = e\hbar B v_D^2/\Delta$. For free electrons, this condition is equivalent to the effective g factor of 2 in $E_s = g\mu_B B$ (Bohr magneton $\mu_B = e\hbar/2m_0$) [11].

In this Letter, we demonstrate experimentally that the conduction and valence bands of Bi₂Se₃ are both, with

a good precision, parabolic (perpendicular to the c -axis) and characterized by approximately the same effective mass. This crucial observation implies a great simplification of the multi-parameter Dirac Hamiltonian [5, 12] commonly used to describe the bands of this material.

The resulting simplified Dirac Hamiltonian differs from that of the genuine quantum electrodynamics system only by relevant (additional) diagonal dispersive terms, and importantly, it remains to be defined by two parameters only: by the bandgap energy 2Δ and velocity parameter v_D . These are directly read from our optical experiments, or alternatively, the v_D parameter may be taken from the measurements of the Bi₂Se₃ Dirac-cone surface states [13]. Remarkably and in contrast to genuine Dirac fermions, the electrons in Bi₂Se₃ approximately follow the rule that their spin splitting is twice the cyclotron energy $E_s = \hbar e B v_D^2/\Delta = 2\hbar\omega_c = 2E_c$. The effective mass, common for carriers in the conduction and valence bands, is thus roughly $m_e = m_h = 2\Delta/v_D^2 = 2m_D$ and the spin splitting expressed in terms of the effective g factor, $g_e = g_h = 2m_0/m_D$. Our simplified view of the bands in Bi₂Se₃ is not perfect (departures are extensively discussed), though it accounts well for the present experimental results as well as for a number of magneto-transport data reported in the past and agrees with the recent estimate of the electron g factor.

The presented experiments have been performed on a 290-nm-thick layer of Bi₂Se₃ grown by molecular beam epitaxy on a semi-insulating InP(111)B substrate [14]; for data obtained on another specimen prepared under analogous conditions see Supplementary materials [15]. The 3D structure of the InP surface (with 2 nm root mean square roughness) transfers the stacking order of

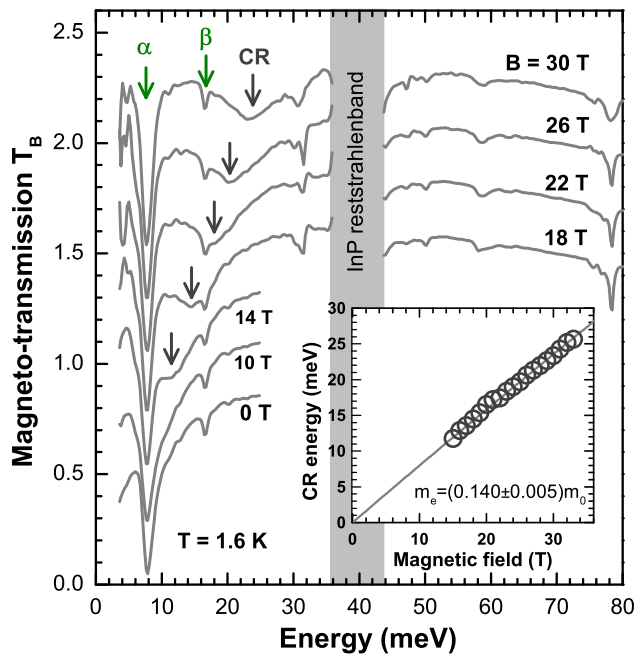


Fig. 1. (color online) Far infrared magneto-transmission spectra of the Bi_2Se_3 specimen. The infrared active phonon modes α and β are at higher magnetic fields accompanied by CR absorption, which follows linear in B dependence, see the inset, and implies the effective mass of electrons $m_e = (0.140 \pm 0.005)m_0$. The plotted transmission T_B was normalized by that of the bare InP substrate.

the substrate to the epilayer, resulting in a complete suppression of twinning, which is otherwise a ubiquitous defect in Bi_2Se_3 thin films. The after-growth annealing in the Se atmosphere, reducing the final density of Se vacancies, helped to keep the electron density below 10^{18} cm^{-3} (with the mobility μ in the $10^3 \text{ cm}^2 \cdot \text{V}^{-1} \cdot \text{s}^{-1}$ range), as confirmed in magneto-transport experiments. Importantly, the thin epitaxial layer of Bi_2Se_3 enabled transmission experiments at photon energies above the fundamental interband absorption edge of this material.

To measure the magneto-transmission spectra, a macroscopic area of the sample ($\sim 4 \text{ mm}^2$) was exposed to the radiation of a globar, which was analysed by a Fourier transform spectrometer and, using light-pipe optics, delivered to the sample placed in a superconducting or resistive magnet. The transmitted light was detected by a composite bolometer placed directly below the sample, kept at a temperature of 1.6 K. All measurements were done in the Faraday configuration with light propagating along the c axis of Bi_2Se_3 (z axis). In experiments performed with circularly polarized light, a glass linear polarizer and a zero-order MgF_2 quarter wave plates (centered at $\lambda = 4$ or $5 \mu\text{m}$) were used.

The optical response of the thin Bi_2Se_3 layer has been probed in both far and middle infrared spectral regions. At low energies, the response, see Fig. 1, is dominated

by infrared active phonon modes α and β , which exhibit a weak coupling to the magnetic field [17]. At higher magnetic fields, cyclotron resonance (CR) absorption is well formed and it disperses linearly with B . The slope of this dependence provides us with an estimate of the electron effective mass: $m_e = (0.140 \pm 0.005)m_0$, which well falls into a relatively broad range of values, $m_e = (0.12 - 0.16)m_0$, deduced from other experiments [18–22]. The interband absorption of Bi_2Se_3 exhibits a fairly rich response in magnetic fields, see Fig. 2(a). Firstly, at low B , a distortion of the absorption edge at the energy slightly above 200 meV appears. At higher fields ($B > 10 \text{ T}$), the quantum regime is approached ($\mu \cdot B > 1$) and a series of interband inter-Landau level (inter-LL) resonances emerges. These resonances are almost equidistant in energy and follow nearly linear in B dependence, see Fig. 2(b).

The observed linearity of the optical response in B , in reference to intraband (CR absorption) as well as interband inter-LL excitations, points towards parabolic profiles of both conduction and valence bands. Let us reconcile this crucial experimental fact with the standard theoretical model of electronic bands in TIs from Bi_2Se_3 family [5, 12]. Using a basis of spin-degenerate Se- and Bi-like p -orbitals, the authors of Refs. [5, 12] propose a 3D Dirac Hamiltonian (4×4), expanded to include the electron-hole asymmetry, uniaxial anisotropy (along the c axis), and importantly, the band inversion, giving thus rise to the TI phase (via dispersive diagonal terms).

Since these are the $k_z = 0$ states, which provide the dominant contribution to the magneto-optical response studied in our experiments, the situation further simplifies. The 3D Dirac Hamiltonian decouples into two complex-conjugate 2D Dirac-type Hamiltonians h and h^* written in the basis of $|\text{Se} \downarrow\rangle$, $|\text{Bi} \uparrow\rangle$ and $|\text{Se} \uparrow\rangle$, $|\text{Bi} \downarrow\rangle$, respectively:

$$h = \begin{pmatrix} \Delta + (C + M)k^2 & \hbar v_D k_+ \\ \hbar v_D k_- & -\Delta + (C - M)k^2 \end{pmatrix}, \quad (1)$$

where $k_{\pm} = k_x \pm ik_y$. This Hamiltonian implies, in general, non-parabolic conduction and valence band profiles:

$$\mathcal{E}_{c,v}(k) = Ck^2 \pm \sqrt{(\Delta + Mk^2)^2 + \hbar^2 v_D^2 k^2}, \quad (2)$$

each exhibiting up to three local extremal points, depending on the strength of the interband coupling v_D (effective speed of light), the electron-hole asymmetry parameter C , and the diagonal dispersive term M (negative for systems with the band inversion). The basis of the h Hamiltonian allows us to associate a given spin projection to each band: $\mathcal{E}_{c\downarrow}$ and $\mathcal{E}_{v\uparrow}$. To satisfy the time-reversal and inversion symmetries of Bi_2Se_3 , the Hamiltonian h^* provides an analogous solution, with the spin projections rotated, $\mathcal{E}_{c\uparrow}$ and $\mathcal{E}_{v\downarrow}$, so we finally obtain twice spin-degenerate conduction and valence bands.

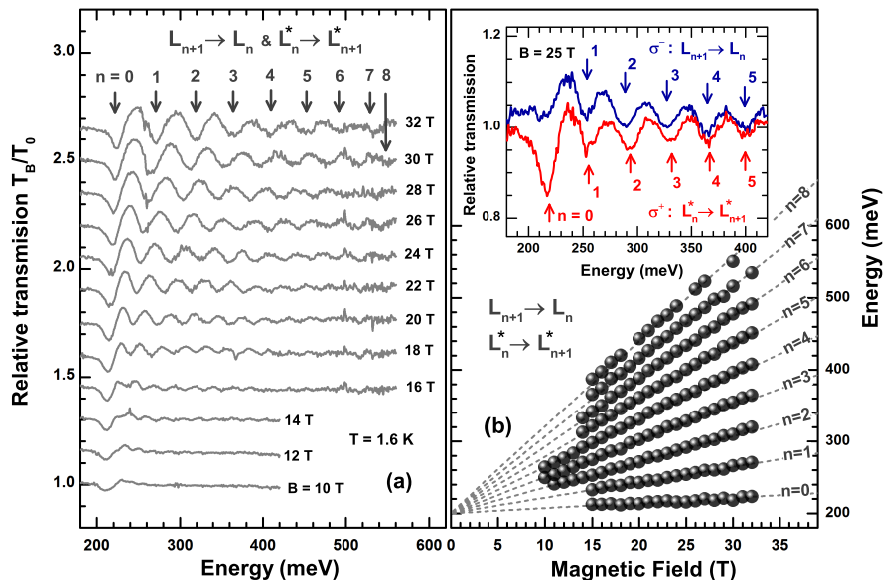


Fig. 2. (color online) Part (a): Relative transmission spectra of Bi_2Se_3 in the middle infrared spectral range plotted for selected values of B . At $B = 32$ T, individual excitations are denoted by vertical arrows and identified by the corresponding index n . Part (b): Positions of experimentally observed interband excitations as a function of B . The dashed lines represent theoretical fit to data described in the text. The inset shows the magneto-transmission spectrum taken at $B = 25$ T measured with a defined circular polarization of light. Notably, it is the normalization by T_0 , which induces the modulation of T_B/T_0 curves around the zero-field interband absorption edge of $\hbar\omega = 2\Delta + E_F(1 + m_e/m_h) \approx 225$ meV.

To make the above dispersions (2) parabolic in a broad range of energies, *i.e.*, to make the model consistent with our magneto-optical data, the specific condition $\hbar^2 v_D^2 = -4M\Delta$ has to be satisfied. Notably, this is only possible for systems in the TI phase when $M < 0$ (by definition $\Delta > 0$). The bands then take a simple form, $\mathcal{E}_c = \Delta + (C - M)k^2$ and $\mathcal{E}_v = -\Delta + (C + M)k^2$, and are characterized by well-defined effective masses: $m_e = \hbar^2/[2(C - M)] = 2\hbar^2/(\hbar^2/m_D + 4C)$ and $m_h = -\hbar^2/[2(C + M)] = 2\hbar^2/(\hbar^2/m_D - 4C)$, for electrons and holes, respectively. Interestingly, the corresponding reduced mass equals to the Dirac mass: $1/m_e + 1/m_h = 1/m_D = v_D^2/\Delta$. Clearly, in the case of a relatively weak electron-hole asymmetry ($C \ll |M|$), the expressions further reduce to $m_e \approx m_h \approx 2m_D$.

When the magnetic field is applied, the bands in Bi_2Se_3 transform into Landau levels (LLs). The Dirac-type Hamiltonians h and h^* give rise to particular electron and hole zero-mode LLs: $E_{0,e} = \Delta + (C + M)eB/\hbar$ and $E_{0,h}^* = -\Delta + (C - M)eB/\hbar$. These zero-mode levels are typical of TIs (see, *e.g.*, Refs. [3]) – they disperse strictly linearly with B , they are spin polarized, insensitive to the strength of the interband coupling v_D and they cross each other at the field of $B_c = \hbar\Delta/|eM|$. The LLs with higher indices ($n > 0$) follow, assuming parabolic bands with a relatively weak electron-hole asymmetry $C \ll |M|$ (a posteriori justified by our experimental data), nearly linear in B dependence. For h and h^* Hamiltonians we get the LL spectrum: $E_{n,e} = E_{0,e} + \hbar\omega_c n$, $E_{n,e}^* = E_{n-1,e} + \hbar\omega_c^D$, $E_{n,h}^* = E_{0,h}^* - \hbar\omega_c^h n$ and $E_{n,h} = E_{n-1,h}^* - \hbar\omega_c^D$, where $\omega_c^{e,h,D} = eB/m_{e,h,D}$.

Importantly, the shift $\hbar\omega_c^D$ between the two LL series corresponds to the spin splitting $E_s = \hbar e B v_D^2/\Delta$, which may be expressed also in terms of a g factor: $g_e = g_h = 2m_0/m_D$, see Supplementary materials [15]. In analogy

to massive particles in quantum electrodynamics, this spin splitting is given just by the energy bandgap (2Δ) and the effective velocity of light (v_D) and it is the same for electrons and holes (particles and antiparticles). On the other hand, the effective masses of electrons and holes depend on the diagonal terms M and C and this implies a certain ratio, $E_s/E_c > 1$, between the cyclotron energy and spin splitting (notably, $E_c/E_s = 1$ always holds for free electrons in vacuum). The spin-splitting of electronic bands in TIs (with $M < 0$) should thus manifest at lower magnetic fields, prior to Landau level quantization cf. Figs. 3(a-c). This, in fact, accounts for the initial distortion of the absorption edge observed at low magnetic fields, see Fig. 2(a). Interestingly, for rather small electron-hole asymmetry ($C \ll |M| \Rightarrow m_e \rightarrow 2m_D$), we get $2E_c = 2\hbar\omega_c = \hbar e B/m_D = g_e \mu_B B = E_s$.

The Dirac Hamiltonian (1) in a magnetic field gives rise to two series of dipole-active inter-LL excitations $n \rightarrow n + 1$ and $n \rightarrow n - 1$, active in σ^+ and σ^- polarized light, respectively. This has been corroborated both experimentally and theoretically, for instance, in the context of graphene [23, 24]. However, a closer look at the corresponding matrix elements shows that, in a gapped system ($\Delta \neq 0$), $n \rightarrow n - 1$ transitions dominate interband inter-LL absorption within the spectrum of the h Hamiltonian, and vice versa, the $n \rightarrow n + 1$ series in the h^* Hamiltonian, see Fig. 3(c) for illustration and Supplementary materials [15] for details. This behavior may be viewed as a spin-dependent optical activity, implying necessity to reverse spin during the interband absorption. The interband excitations, $\mathcal{E}_{v\downarrow} \rightarrow \mathcal{E}_{c\uparrow}$ and $\mathcal{E}_{v\uparrow} \rightarrow \mathcal{E}_{c\downarrow}$, connecting states within h^* or h Hamiltonians, respectively, are thus active in σ^+ and σ^- polarized radiation only. Notably, a similar situation is encountered in gapped graphene and transition-metal dichalcogenides,

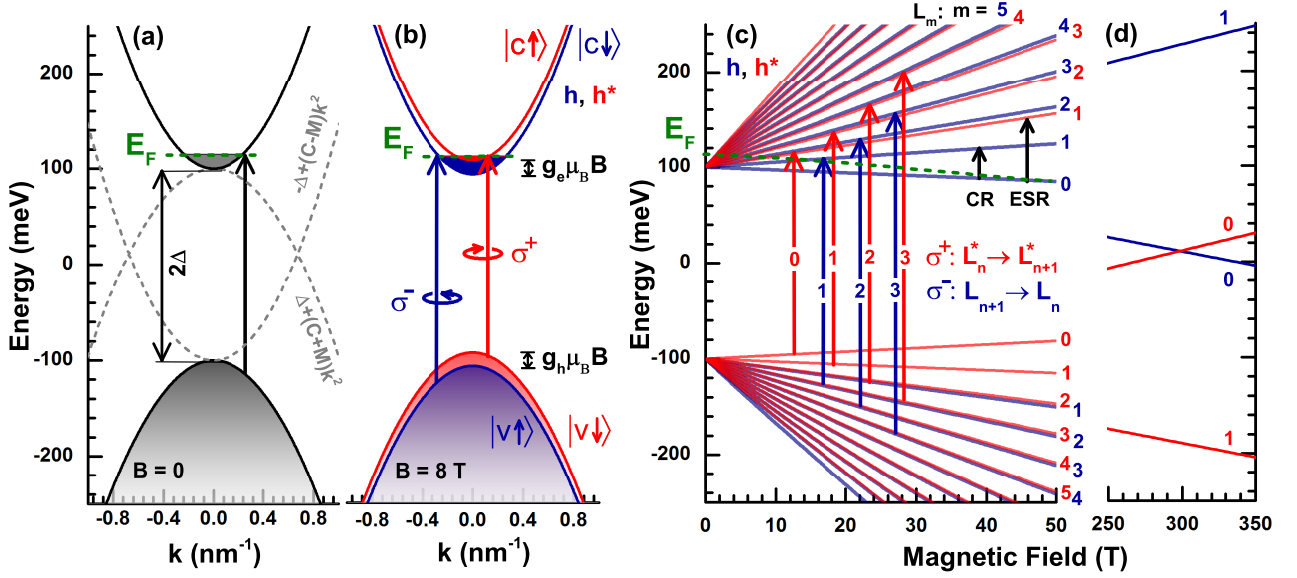


Fig. 3. (color online) Part (a): Approximate profile of electronic bands in Bi_2Se_3 at the center of the Brillouin zone (for $k_z = 0$). The dashed lines show the (dispersive) diagonal term of the Hamiltonian (1). Part (b): Spin splitting of the conduction and valence bands ($g_e \approx g_h$) at $B = 8$ T (LLs not yet resolved $\mu_B < 1$). Part (c): Fan chart of nearly linear in B LLs in Bi_2Se_3 . The approximate match of LLs $E_{n+1,e} \approx E_{n,e}^*$ & $E_{n,h} \approx E_{n+1,h}^*$ is a direct consequence of the Dirac-type model for electronic states in Bi_2Se_3 discussed in the text. Vertical arrows show selected electric-dipole-active interband inter-LL resonances, CR absorption as well as (expected) magnetic-dipole-active electron spin resonance (ESR) absorption in the quantum limit. Part (d): High-magnetic-field extrapolation of zero-mode LLs, with the crossing point at $B_c \approx 300$ T.

where valley-sensitive selection rules for circularly polarized light appear [25]. Let us also note that intraband (CR) absorption is always active in σ^+ and σ^- polarized radiation for electrons and holes, respectively.

The LL spectrum and the selection rules allows us to identify individual resonances in the interband response in Fig. 2. When the quantum limit is reached ($B > 20$ T), the lowest in energy observed absorption line is the $L_0^* \rightarrow L_1^*$ transition, active in σ^+ polarized light. The parent $L_1 \rightarrow L_0$ line, active in σ^- polarized radiation, does not appear, since the bottom of E_0 level is always occupied in the n doped system, cf. the inset of Fig. 2(b) and Fig. 3(c). At higher energies, we get a series of transitions, $L_n^* \rightarrow L_{n+1}^*$ and $L_{n+1} \rightarrow L_n$ ($n > 0$), which are for a given n nearly degenerate in energy and active in σ^+ and σ^- polarized light, respectively. Their spacing, $\hbar(\omega_c^e + \omega_c^h) = \hbar\omega_c^D$, allows us to read the Dirac mass directly from the data: $m_D = (0.080 \pm 0.005)m_0$. Notably, this Dirac mass implies $g_e = g_h = 2m_0/m_D \approx 25$, which is in very good agreement with the value $g_e^{\text{ESR}} = 27.5$ [26], derived recently using spin resonance measurements. The Dirac mass m_D , together with the bandgap $2\Delta = (200 \pm 5)$ meV, read from the low-field extrapolation of interband inter-LL resonances in Fig. 2(b), imply the velocity $v_D = \sqrt{\Delta/m_D} = 4.8 \times 10^5$ m/s, in perfect agreement with majority of ARPES studies [13, 27].

Comparing the estimated Dirac mass with the electron mass (as deduced from CR absorption), we conclude that

$m_e \approx 2m_D$. This indicates rather weak electron-hole asymmetry in Bi_2Se_3 ($C \ll |M| = \hbar^2 v_D^2 / 4\Delta$). Neglecting this asymmetry completely, we remain with the Hamiltonian (1) with two independent parameters only: Δ and v_D . Interestingly, these two parameters, which can be easily read from infrared transmission experiments, fully describe the band structure of Bi_2Se_3 : the energy bandgap of 2Δ , effective masses $m_e \approx m_h \approx 2m_D = 2\Delta/v_D^2$, as well as g factors, $g_e = g_h = 2m_0/m_D = 2m_0 v_D^2 / \Delta$. Notably, this match between twice cyclotron energy and spin splitting ($2\hbar eB/m_e = g_e \mu_B B$) has been in the past found as a purely empirical fact in quantum oscillation experiments on Bi_2Se_3 , see, *e.g.*, Refs. [28, 29]. Here we show that this surprising match is not accidental and it straightforwardly follows from the Dirac-type Hamiltonian (1) applied to TI with a weak electron-hole asymmetry and nearly parabolic bands.

It should be also mentioned that within our “parabolic view” of electronic bands, Bi_2Se_3 clearly becomes a direct-gap semiconductor. This is in agreement with recent experimental (ARPES) and theoretical studies, see, *e.g.*, Refs. [30–33], however, in contradiction with other ARPES data, see, *e.g.*, Refs. [13, 27], in which the observed camel-back profile of the valence band indicated an indirect band gap. Intriguingly, our experiments, together with other optical studies performed on bulk or thin-film specimens, see, *e.g.*, Refs. [34–36], provide a significantly lower band gap (200 meV) as compared to

values deduced from ARPES experiments (~ 300 meV), see Supplementary materials [15] for further discussions. Now we will discuss the limits of our simplified two-parameter model (with parabolic bands and full electron-hole symmetry), by confronting it with more detailed analysis of our experimental data. The real band structure of Bi_2Se_3 may deviate by (i) appearance of the electron-hole asymmetry and (ii) the departure of bands from exact parabolicity. The electron-hole asymmetry is clearly demonstrated by $m_e < m_h$ ($m_e < 2m_D$), which translates into $C = (3 \pm 0.5)$ eV.Å², but also by the difference in the corresponding g factors. The latter may be read from a small, but noticeable, splitting between $L_n^* \rightarrow L_{n+1}^*$ and $L_{n+1} \rightarrow L_n$ transitions in the spectra taken with a defined circular polarization of light, see the inset of Fig. 2(b). It implies $g_e - g_h \approx 3$, which may be explained as the contribution of the free-electron Zeeman term and influence of remote bands, described by, *e.g.*, the Roth's formula [12, 37].

The deviations from bands' parabolicity imply the departure of inter-LL resonances from their linearity in B . Indeed, the transitions at higher energies and/or for higher LL indices, see Fig. 2(b), slow down to a weak sublinear dependence. To describe this behavior, we have used the full (non-linearized) expressions for LLs, see Supplementary materials [15], to fit the positions of individual resonances. We varied parameters v_D , M and Δ , while fixing $C \equiv 0$, which has rather weak impact on the interband response. The best agreement is obtained for $v_D = (0.47 \pm 0.02) \times 10^6$ m.s⁻¹, $\Delta = (0.100 \pm 0.002)$ eV and $M = -(22.5 \pm 1.0)$ eV.Å². We may thus conclude that the condition $\hbar^2 v_D^2 = -4M\Delta$ is fulfilled within a few percent, which validates our view of parabolic bands in Bi_2Se_3 . Moreover, since $C/|M| \sim 1/10$, the system indeed exhibits rather high electron-hole symmetry.

The deduced strength of dispersive diagonal terms, M and Δ , allows us to estimate the critical field B_c , at which the zero-mode LLs cross each other, see Fig. 3(d). At this magnetic field, Bi_2Se_3 changes into a semi-metallic (= gapless) material, for which the extended 3D Dirac Hamiltonian implies, see Supplementary materials [15], the linear in k_z bands, $E(k_z) = \pm \hbar \tilde{v}_D |k_z|$, with a high (LL) degeneracy $\zeta = eB/\hbar$. The velocity \tilde{v}_D is supposed to be slightly lower as compared to v_D due to the uniaxial anisotropy of Bi_2Se_3 [18, 29]. The pretty high value of $B_c \approx 300$ T, at the limit of currently available (semi-destructive) pulsed-field techniques [38], makes the exploration of this interesting critical point difficult. However, this crossing field B_c is expected to be lower in other TIs from the Bi_2Se_3 family, with a lower band gap, *e.g.*, in $\text{Bi}_{1-x}\text{Sb}_x$ for rather low Sb concentrations [4].

In conclusion, we have shown that the band structure of Bi_2Se_3 can be, in very good approximation, described by a simple Dirac-type Hamiltonian with only two free parameters: the effective velocity parameter v_D and the band gap 2Δ . This simplified model provides us with

reasonable estimates for both effective masses ($m_e \approx m_h \approx 2\Delta/v_D^2$) and corresponding g factors ($g_e \approx g_h \approx 2m_0 v_D^2/\Delta$), and implies, for charge carriers in Bi_2Se_3 , a surprising match between the cyclotron energy and spin-splitting: $E_s \approx 2E_c$. Notably, this relation has been deduced from quantum oscillations experiments performed on Bi_2Se_3 in the past, but only as a purely empirical fact. Here we show that this directly follows from the Dirac-type Hamiltonian applied to a TI with nearly parabolic bands and a high electron-hole symmetry.

The work has been supported by the ERC-AG projects MOMB and 3-TOP. Authors acknowledge discussions with D. M. Basko, O. Ly and M. O. Goerbig. T. B. acknowledges the support from the Austrian Science Fund (FWF), Grant No. M 1603-N27. E. M. H. and C. M. thank DFG grant HA 5893/4-1 within SPP 1666.

* milan.orlita@lncmi.cnrs.fr

- [1] K. S. Novoselov *et al.*, Nature **438**, 197 (2005).
- [2] Y. B. Zhang *et al.*, Nature **438**, 201 (2005).
- [3] B. A. Bernevig and S.-C. Zhang, Phys. Rev. Lett. **96**, 106802 (2006); M. König *et al.*, Science **318**, 766 (2007).
- [4] D. Hsieh *et al.*, Nature **452**, 970 (2008).
- [5] H. Zhang *et al.*, Nature Phys. **5**, 438 (2009).
- [6] M. Z. Hasan and C. L. Kane, Rev. Mod. Phys. **82**, 3045 (2010); X.-L. Qi and S.-C. Zhang, Rev. Mod. Phys. **83**, 1057 (2011).
- [7] Z. K. Liu *et al.*, Science **343**, 864 (2014).
- [8] M. Orlita *et al.*, Nature Phys. **10**, 233 (2014).
- [9] Z. K. Liu *et al.*, Nature Mater. **13**, 677 (2014).
- [10] W. Zawadzki, Adv. Phys. **23**, 435 (1974).
- [11] V. B. Berestetskii, E. M. Lifshitz, and L. P. Pitaevskii, "A course of theoretical physics, vol. 3, p. 455," (Pergamon, 1977).
- [12] C.-X. Liu *et al.*, Phys. Rev. B **82**, 045122 (2010).
- [13] Y. Xia *et al.*, Nature Phys. **5**, 398 (2009).
- [14] N. V. Tarakina *et al.*, Adv. Mater. Int. **1**, 1400134 (2014).
- [15] See Supplemental Materials.
- [16] O. B. O. Ly, *Electron spin resonance in topological insulators: Theoretical study*, Master's thesis, Université de Strasbourg (2014).
- [17] A. D. LaForge *et al.*, Phys. Rev. B **81**, 125120 (2010).
- [18] H. Köhler and E. Wöchner, phys. stat. sol. (b) **67**, 665 (1975); K. Eto *et al.*, Phys. Rev. B **81**, 195309 (2010).
- [19] J. G. Analytis *et al.*, Phys. Rev. B **81**, 205407 (2010).
- [20] N. P. Butch *et al.*, Phys. Rev. B **81**, 241301 (2010).
- [21] A. N. Sushkov *et al.*, Phys. Rev. B **82**, 125110 (2010).
- [22] H. Cao *et al.*, Phys. Rev. Lett. **108**, 216803 (2012).
- [23] M. L. Sadowski *et al.*, Phys. Rev. Lett. **97**, 266405 (2006).
- [24] V. P. Gusynin, S. G. Sharapov, and J. P. Carbotte, Phys. Rev. Lett. **98**, 157402 (2007).
- [25] W. Yao, D. Xiao, and Q. Niu, Phys. Rev. B **77**, 235406 (2008); F. Rose, M. Goerbig, and F. Piéchon, *ibid.* **88**, 125438 (2013).
- [26] A. Wolos *et al.*, AIP Conf. Proc. **1566**, 197 (2013).
- [27] Z.-H. Zhu *et al.*, Phys. Rev. Lett. **107**, 186405 (2011).
- [28] H. Köhler and H. Fischer, phys. stat. sol. (b) **69**, 349 (1975).

- [29] B. Fauqué *et al.*, Phys. Rev. B **87**, 035133 (2013).
 [30] Y. L. Chen *et al.*, Science **329**, 659 (2010).
 [31] O. V. Yazyev *et al.*, Phys. Rev. B **85**, 161101 (2012).
 [32] I. Aguilera *et al.*, Phys. Rev. B **88**, 045206 (2013).
 [33] I. A. Nechaev *et al.*, Phys. Rev. B **87**, 121111 (2013).
 [34] D. Greenaway and G. Harbeke, J. Phys. Chem. Solids **26**, 1585 (1965).
 [35] H. Köhler and J. Hartmann, phys. stat. sol. (b) **63**, 171 (1974).
 [36] K. W. Post *et al.*, Phys. Rev. B **88**, 075121 (2013).
 [37] L. M. Roth, B. Lax, and S. Zwerdling, Phys. Rev. **114**, 90 (1959).
 [38] O. Portugall *et al.*, C. R. Phys. **14**, 115 (2013), and references therein.

Supplementary Information for

Magneto-optics of massive Dirac fermions in bulk Bi₂Se₃

by M. Orlita, B. A. Piot, G. Martinez, N. K. Sampath Kumar, C. Faugeras, M. Potemski,
 C. Michel, E. M. Hankiewicz, T. Brauner, Č. Drašar,
 S. Schreyeck, S. Grauer, K. Brunner, C. Gould, C. Brüne, and L. W. Molenkamp

In this supplementary material, we present details of Landau level (LL) spectrum and optical selection rules for bulk Bi₂Se₃.

BULK LANDAU LEVELS

Liu *et al.* proposed a 3D Dirac Hamiltonian to describe the bulk states in Bi₂Se₃ [S1,S2]. This Hamiltonian, written in the basis $\{|\text{Se} \downarrow\rangle, |\text{Bi} \uparrow\rangle, |\text{Se} \uparrow\rangle, |\text{Bi} \downarrow\rangle\}$, reads:

$$\mathcal{H} = \epsilon(\mathbf{k})\mathbf{1}_{4 \times 4} + \begin{pmatrix} \mathcal{M}(\mathbf{k}) & \mathcal{A}(k)k_+ & 0 & -\mathcal{B}(k_z)k_z \\ \mathcal{A}(k)k_- & -\mathcal{M}(\mathbf{k}) & \mathcal{B}(k_z)k_z & 0 \\ 0 & \mathcal{B}(k_z)k_z & \mathcal{M}(\mathbf{k}) & \mathcal{A}(k)k_- \\ -\mathcal{B}(k_z)k_z & 0 & \mathcal{A}(k)k_+ & -\mathcal{M}(\mathbf{k}) \end{pmatrix}, \quad (3)$$

where $\epsilon(\mathbf{k}) = C_0 + C_1k_z^2 + C_2k^2$, $\mathcal{M}(\mathbf{k}) = M_0 + M_1k_z^2 + M_2k^2$, $\mathcal{B}(k_z) = B_0 + B_2k_z^2$, $\mathcal{A}(k) = A_0 + A_2k^2$, $k_{\pm} = k_x \pm ik_y$ and $k^2 = k_x^2 + k_y^2$. In the simplified model, employed in the main text, we restrict this Hamiltonian by neglecting the k^3 terms and redefine $\Delta \equiv M_0$, $M \equiv M_2$, $C \equiv C_2$, $C_0 \equiv 0$ and $v_D = A_0/\hbar$.

To examine the Landau level structure, we introduce the magnetic field (along the z axis) by means of the Peierls substitution $\mathbf{k} \rightarrow \boldsymbol{\pi} := \mathbf{k} + \frac{e\mathbf{A}}{\hbar}$, where \mathbf{A} is the vector potential, $\mathbf{B} = \nabla \times \mathbf{A}$ and $\mathbf{B} \parallel \mathbf{z}$. In the quantizing magnetic fields, the LL spectrum of electrons and holes takes the form of $E_{n,e}(k_z)$ and $E_{n,h}(k_z)$. The inversion symmetry of the system implies: $E_{n,e/h}(k_z) = E_{n,e/h}(-k_z)$ and therefore $dE_{n,e/h}/dk_z = 0$ at $k_z = 0$. This induces a series of singularities in the density of states for electrons and holes, but importantly for our case, also in the joint density of states (for each LL and inter-LL resonance, respectively). Using a parabolic expansion in k_z (approximately valid for $k_z \approx 0$), we get the characteristic $\rho_{e-h}(\omega) \propto 1/\sqrt{\hbar\omega - E}$ profiles in the vicinity of each resonance in the joint density of states. Such a profile is typical of 1D systems with a parabolic dispersion. The singularities in ρ_{e-h} , in reality smoothed by disorder, give rise to the experimentally observed inter-LL resonances. In principle, more complex Landau level profiles in the momentum k_z may provide further singularities/resonances (due to states at $k_z \neq 0$), nevertheless, we did not identify any such transitions in our magneto-transmission spectra. The magneto-optical response of Bi₂Se₃ ($\mathbf{B} \parallel \mathbf{z}$) is thus dominantly determined by $k_z = 0$ states.

For $k_z = 0$, the 3D Hamiltonian (3) reduces to two 2D Dirac-like Hamiltonians:

$$\mathcal{H}_0 = \begin{pmatrix} h_0(\boldsymbol{\pi}) & 0 \\ 0 & h_0^*(\boldsymbol{\pi}) \end{pmatrix} \quad \text{with} \quad h_0(\boldsymbol{\pi}) = \epsilon(\boldsymbol{\pi})\mathbf{1}_{2 \times 2} + \begin{pmatrix} \mathcal{M}(\boldsymbol{\pi}) & A_0\boldsymbol{\pi}_+ \\ A_0\boldsymbol{\pi}_- & -\mathcal{M}(\boldsymbol{\pi}) \end{pmatrix}, \quad (4)$$

that will be referred to as the ‘‘full model’’ in the following discussion. Now, without k_z terms, we have $\epsilon(\boldsymbol{\pi}) = C\boldsymbol{\pi}^2$, where C breaks the particle-hole symmetry. $\mathcal{M}(\boldsymbol{\pi})$ is the k dependent mass term $\mathcal{M}(\boldsymbol{\pi}) = \Delta + M\boldsymbol{\pi}^2$ with Δ determining the band gap $E_g = 2\Delta$ at $k = 0$.

To study the formation of LLs, we introduce the ladder operators:

$$a = \frac{l_B}{\sqrt{2}}\boldsymbol{\pi}_-, \quad a^\dagger = \frac{l_B}{\sqrt{2}}\boldsymbol{\pi}_+, \quad (5)$$

with the magnetic length $l_B = \sqrt{\frac{\hbar}{eB}}$. These operators obey the standard relations $[a, a^\dagger] = 1$, $a|n\rangle = \sqrt{n}|n-1\rangle$ and $a^\dagger|n\rangle = \sqrt{n+1}|n+1\rangle$. Using the definitions (5), we can rewrite $h_0(\boldsymbol{\pi})$ in terms of the raising and lowering operators:

$$h_0(a^\dagger, a) = \begin{pmatrix} \Delta + \frac{2}{l_B^2}(C+M)(a^\dagger a + \frac{1}{2}) & \frac{\sqrt{2}}{l_B} A_0 a^\dagger \\ \frac{\sqrt{2}}{l_B} A_0 a & -\Delta + \frac{2}{l_B^2}(C-M)(a^\dagger a + \frac{1}{2}) \end{pmatrix}. \quad (6)$$

The form of this Hamiltonian suggests the following ansatz for the eigenstates:

$$\Phi_{n \neq 0} = \begin{pmatrix} c_{n1} |n\rangle \\ c_{n2} |n-1\rangle \end{pmatrix} \quad \text{and} \quad \Phi_0 = \begin{pmatrix} |0\rangle \\ 0 \end{pmatrix} \quad \text{with} \quad \langle n|m\rangle = \delta_{nm}. \quad (7)$$

Solving the Schrödinger equation, we find the LL spectrum:

$$E_{n,\alpha} = \frac{M}{l_B^2} + 2\frac{C}{l_B^2}n + s_\alpha \sqrt{\left(\frac{C}{l_B^2} + \Delta + 2\frac{M}{l_B^2}n\right)^2 + 2\frac{A_0^2}{l_B^2}n}, \quad (8)$$

$$E_{0,e} = \Delta + \frac{C+M}{l_B^2},$$

where $s_e = +1$ for electrons and $s_h = -1$ for holes. Note that each state with the energy of $E_{n \geq 1, \alpha}$ is always a superposition of the $|\text{Se}, n, \downarrow\rangle$ level and the $|\text{Bi}, n-1, \uparrow\rangle$ level. In contrast, the $E_{0,e}$ state is fully polarized as a $|\text{Se}, \downarrow\rangle$ level. The presence of such polarized zero-mode LLs is characteristic of Dirac-type Hamiltonians and it is well-known, *e.g.*, from physics of graphene [S3]. However, in graphene, the zero-mode levels (at K and K' points) are polarized in pseudospin not in real spin as in the case of Bi_2Se_3 .

The Landau levels for the h_0^* Hamiltonian are found in an analogous way. Here, we take

$$\Phi_{n \neq 0}^* = \begin{pmatrix} c_{n1^*} |n-1\rangle \\ c_{n2^*} |n\rangle \end{pmatrix} \quad \text{and} \quad \Phi_0^* = \begin{pmatrix} 0 \\ |0\rangle \end{pmatrix} \quad \text{with} \quad \langle n|m\rangle = \delta_{nm} \quad (9)$$

as the ansatz for the eigenstates and get LLs for the h_0^* Hamiltonian:

$$E_{n,\alpha}^* = -\frac{M}{l_B^2} + 2\frac{C}{l_B^2}n + s_\alpha \sqrt{\left(\frac{C}{l_B^2} - \Delta - 2\frac{M}{l_B^2}n\right)^2 + 2\frac{A_0^2}{l_B^2}n}, \quad (10)$$

$$E_{0,h}^* = -\Delta + \frac{C-M}{l_B^2}.$$

Note that “*” just denotes energies/states belonging to the h_0^* Hamiltonian and does not stand for complex conjugation. We will keep this notation in the next sections. For the h_0^* Hamiltonian, the state with the energy $E_{n \geq 1, \alpha}$ is always a superposition of the $|\text{Se}, n-1, \uparrow\rangle$ level and the $|\text{Bi}, n, \downarrow\rangle$ level. Again, the zero-mode LL is fully spin-polarized, in this case as a $|\text{Bi}, \downarrow\rangle$ state.

The LL spectrum of the Hamiltonian (4) (calculated within the full model) is plotted in Fig. 4 for parameters derived from our magneto-optical experiments, together with electric-dipole transitions discussed later on in detail.

To simplify the LL spectra of the h_0 and h_0^* Hamiltonians, we assume perfectly parabolic bands ($A_0^2 = \hbar^2 v_D^2 = -4M\Delta$) and expand Eq. (8) and Eq. (10) for small magnetic fields. This way we get LLs strictly linear in the applied magnetic field:

$$\begin{aligned} E_{n,e} &= E_{0,e} + \hbar\omega_c^e n, \\ E_{n+1,e}^* &= E_{n,e} + \hbar\omega_c^D, \\ E_{n+1,h} &= E_{n,h}^* - \hbar\omega_c^D, \\ E_{n,h}^* &= E_{0,h}^* - \hbar\omega_c^h n, \end{aligned} \quad (11)$$

where the cyclotron frequencies are defined as $\omega_c^{e/h} = eB/m_{e/h}$ and $\omega_c^D = eB/m_D$ with the effective masses $m_{e/h} = 2\hbar^2 / (\hbar^2/m_D \pm 4C)$ and the Dirac mass $m_D = \Delta/v_D^2$, respectively. Importantly, for parameters deduced from our experimental data, this simplified LL spectrum is nearly identical to that calculated within the full model, see Fig. 5. Further information about Landau levels may be obtained from the analysis of individual eigenstates, which (with the exception of zero-mode levels) represent a superposition of spin-up and spin-down states in the conduction and valence

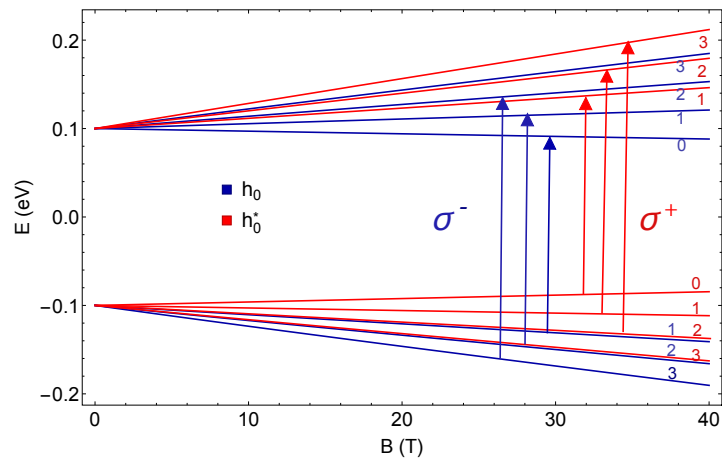


Fig. 4. The Landau level spectrum of the full model (4). Blue levels originate from the h_0 sub-Hamiltonian, red levels from the h_0^* Hamiltonian. The arrows show the dominant type of electric-dipole transitions for the respective Hamiltonian.

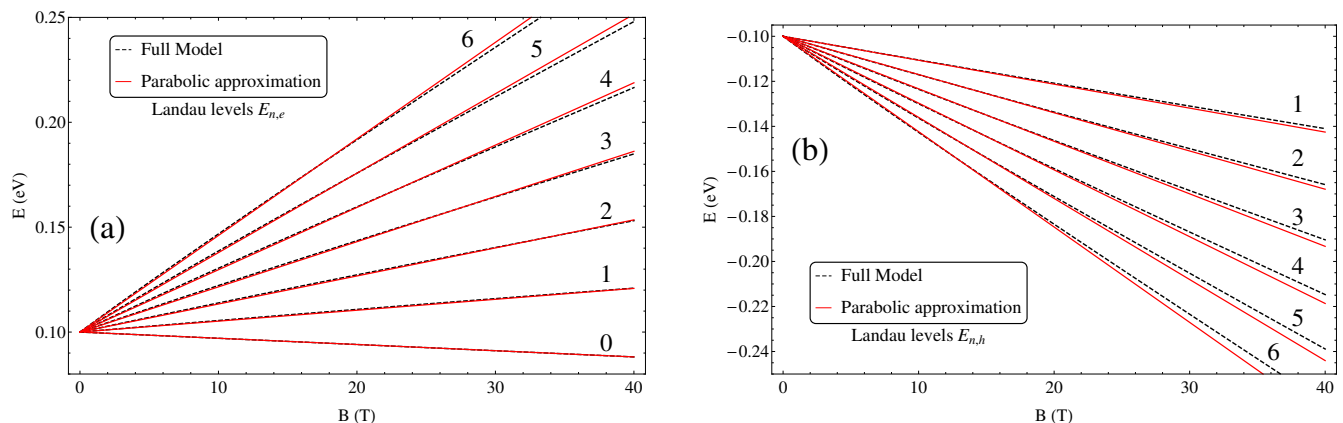


Fig. 5. LLs calculated within the full model, Eq. (8) and (10), compared to LLs obtained by expansion of the same formulas for small magnetic field (*i.e.*, by linearization in B), see Eq. (11). Significant deviations appear only at high magnetic fields and high LL indices. For simplicity, only the levels of the h_0 Hamiltonian are shown.

bands. Nevertheless, for low-energy/low index levels we may always find the dominant state in this superposition, see Fig. 6. We may conclude that the eigenstates of the h_0 Hamiltonian with the energies of $E_{n,e}$ and $E_{n,h}$ can be considered as selenium-like spin-down ($E_n^{\text{Se}\downarrow}$) and bismuth-like spin-up ($E_{n-1}^{\text{Bi}\uparrow}$) levels, respectively. Analogously, states with the energies of $E_{n,e}^*$ and $E_{n,h}^*$ have Se-like spin-up ($E_{n-1}^{\text{Se}\uparrow}$) and bismuth-like spin-down ($E_n^{\text{Bi}\downarrow}$) character, respectively. This assignment of spin-projections will facilitate the definition of g factors in the next section.

DEFINITION OF G FACTORS

For $B = 0$ T the energy states in our system are spin degenerate as required by time- and inversion- symmetry of Bi_2Se_3 . When the magnetic field is applied, this spin degeneracy of states is lifted due to the magnetic moment $\boldsymbol{\mu}$ of electrons. This splitting may be described by a corresponding effective g factor in the Zeeman term, $E_Z = -\boldsymbol{\mu}\mathbf{B}$, with $\boldsymbol{\mu} = g\mu_B\mathbf{s}/\hbar$. The total g factor comprises three contributions. As shown in our experiments, and by the subsequent data analysis, the main contribution results from the strong spin-orbit coupling in Bi_2Se_3 , which is inherently included within the Hamiltonian (3). Further (minor) corrections come from the free electron $g_0 \approx 2$ factor (free-electron Zeeman term) and a perturbative contribution from remote energy bands [S4].

From the previous section, we know that, for small level indices n and low energies, LLs are nearly spin polarized.

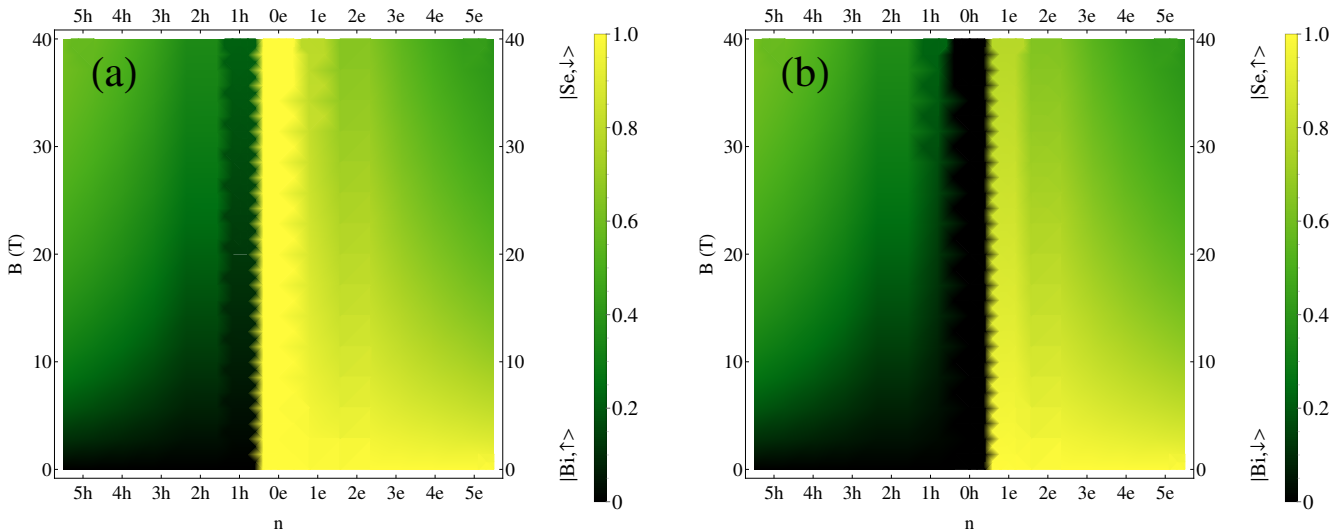


Fig. 6. Probability density of the energy states being Bi-like (dark color) or Se-like (light color) with corresponding spin-polarization. ne and nh denote the LL with index n for electron (e) or hole (h) states. This probability is shown in the part (a) for LLs belonging to the h_0 Hamiltonian, where these levels are a mixture of $|Se, \downarrow\rangle$ and $|Bi, \uparrow\rangle$ states. The part (b) shows this probability for the h_0^* Hamiltonian, where LLs are a mixture of $|Se, \uparrow\rangle$ and $|Bi, \downarrow\rangle$ states. Apart from the zero-mode LLs, one can see that the spin-polarization becomes weaker with increasing magnetic field. However for magnetic fields $B \lesssim 40$ T and low level indices the dominant spin polarization of the energy states stays the same as in the $B \rightarrow 0$ T limit.

In addition, the Landau levels in the valence and conduction bands are bismuth- and selenium-like, respectively. Following this fact, we can express the g factors of charge carriers, in the conduction (c) and valence (v) bands, in terms of LLs calculated from the Hamiltonian Eq. (4):

$$g_c = g_e = g_{Se}(n, B) = (E_n^{Se\uparrow} - E_n^{Se\downarrow})/(\mu_B B) = (E_{n+1,e}^* - E_{n,e})/(\mu_B B), \quad (12a)$$

$$g_v = -g_h = g_{Bi}(n, B) = (E_n^{Bi\uparrow} - E_n^{Bi\downarrow})/(\mu_B B) = (E_{n+1,h} - E_{n,h}^*)/(\mu_B B). \quad (12b)$$

This definition of the $g_{e/h}$ factors for electrons and holes is consistent with magnetic-dipole selection rules: $n \rightarrow n \pm 1$, which interconnect states belonging to the h_0 and h_0^* Hamiltonians [S5]. In addition, we may crosscheck this definition by taking genuine Dirac particles (electrons) in the vacuum. For this, we have to take $A_0 = \hbar c$ ($v_D = c$), $\Delta = m_0 c^2$ and $M = C = 0$, where c is the speed of light and m_0 the rest mass of a free electron. Indeed, we get $g_0 = 2$ as expected.

The definition (12) implies g factors that, in general, depend on the magnetic field as well as on the LL index. However, within our parabolic approximation ($\hbar^2 v_D^2 = -4M\Delta$) and for LLs linearized in B , see Eq. (11), the spin-splitting of electrons and holes becomes linear in magnetic field, $E_s = \hbar\omega_c^D$, implying thus $g_c = -g_v = g_e = g_h = 2m_0/m_D = 2m_0 v_D^2/\Delta$. For the experimentally determined Dirac mass $m_D = (0.080 \pm 0.005)m_0$ we get $g_e = g_h \approx 25$.

Assuming the parabolic approximation ($\hbar^2 v_D^2 = -4M\Delta$), but taking the full expressions for Landau levels (8) and (10), *i.e.*, not linearized in B , the g factors for electrons and holes slightly differ and also gain a weak magnetic-field and Landau-level-index dependence, see Fig. 7. Nevertheless, this is not sufficient to account for the experimentally observed difference, $g_e - g_h \approx 3$, derived from our data in the main text. This may only be explained by further corrections (the Zeeman term with the free-electron $g_0 = 2$ factor and the influence of remote bands).

ZERO-MODE LANDAU LEVELS IN HIGH MAGNETIC FIELDS

In high magnetic fields, the spin-polarized zero-mode LLs $E_{e,0} = \Delta + (C + M)/l_B^2$ and $E_{h,0} = -\Delta + (C - M)/l_B^2$ approach each other and become well separated from the rest of levels. In such a case, we can describe them by an effective Hamiltonian:

$$\mathcal{H}_{\text{zero-mode}} = \begin{pmatrix} E_{e,0} & -\hbar\tilde{v}_D k_z \\ -\hbar\tilde{v}_D k_z & E_{h,0} \end{pmatrix}, \quad (13)$$

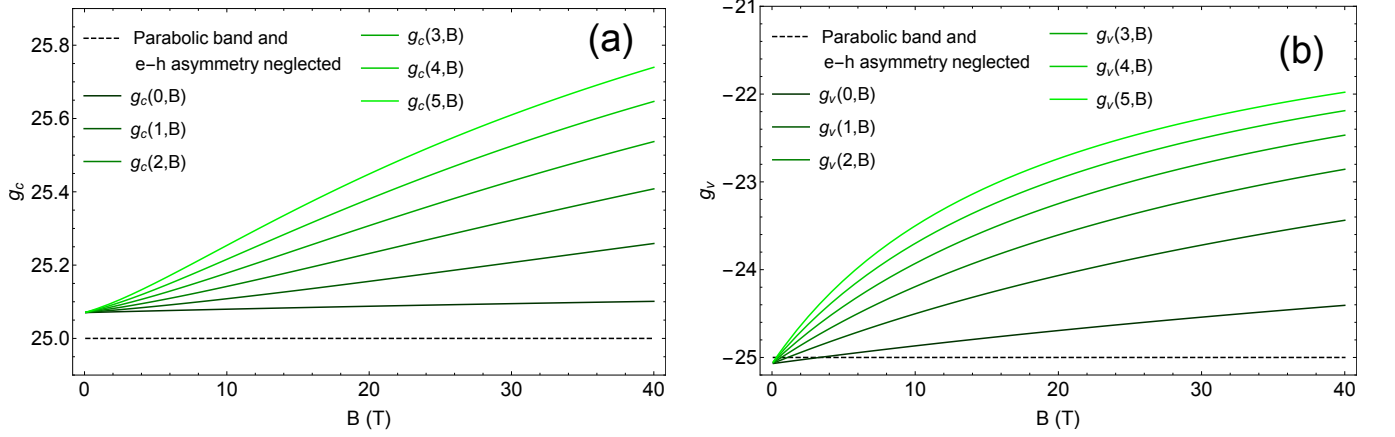


Fig. 7. g factor for charge carriers in the conduction and valence bands, $g_c(n, B)$ and $g_v(n, B)$, exhibiting a weak dependence on the level index n and the magnetic field strength B according to equations (12a) and (12b). (a) With $n \leq 5$ and $B \leq 40$ T the approximate constant value for g_c shows a deviation of $\lesssim 3\%$ from the n - and B -dependent g factor. (b) For g_v this deviation grows to $\lesssim 12\%$. Let us note that we use the notation $g_c = g_e$ and $g_v = -g_h$.

which can be derived from the (k_z dependent) 3D Dirac Hamiltonian (3), proposed in Refs. [S1,S2], in which we neglect the terms cubic in k , terms square in k_z and introduce the magnetic field via Peierls substitution. Taking account of the experimentally observed uniaxial anisotropy of Bi_2Se_3 [S6,S7], one can assume that $\tilde{v}_D = B_0/\hbar \lesssim v_D$. The effective Hamiltonian (13) is equivalent to a 1D Dirac-type Hamiltonian with the band gap of $E_{e,0} - E_{h,0}$. This gap vanishes at the crossing field $B_c = \hbar\Delta/|eM| \approx 300$ T, when the system changes from a (narrow gap) semiconductor into a gapless semimetal. The electronic bands in such a semimetal are equivalent to the 1D Dirac-type channel, $E(k_z) = \pm\hbar\tilde{v}_D|k_z|$ with a strong (LL) degeneracy of states eB/\hbar .

SELECTION RULES AND MATRIX ELEMENTS

To describe the response of our system to an externally applied electromagnetic field, we employ the standard (linear-response) Kubo-Greenwood formalism. For σ^\pm polarized radiation, the optical conductivity tensor, in a system with eigenstates $|\Psi_n\rangle$ and corresponding energies E_n , reads:

$$\sigma_\pm(\omega, B) \propto i \frac{B}{\omega} \sum_{n,n'} \left((f_n - f_{n'}) \frac{|\langle \Psi_{n'} | \hat{v}_\pm(B) | \Psi_n \rangle|^2}{E_n - E_{n'} - \hbar\omega + i\gamma} \right), \quad (14)$$

where f_n is the occupation factor, γ the phenomenological broadening parameter and \hat{v}_\pm the velocity operators. The matrix elements $\langle \Psi_{n'} | \hat{v}_\pm(B) | \Psi_n \rangle$ determine the active electric-dipole transitions (selection rules) between different eigenstates.

The velocity operator can be directly obtained from Eq. (4) by calculating $\hat{v}_i = \frac{1}{\hbar} \frac{\partial H_0}{\partial \pi_i}$, where $i = x, y$ and $v_\pm = (v_x \pm iv_y)/\sqrt{2}$:

$$\hat{v}_+ = \begin{pmatrix} \frac{2(C+M)}{\hbar l_B} a^\dagger & 0 & 0 & 0 \\ \sqrt{2} v_D & \frac{2(C-M)}{\hbar l_B} a^\dagger & 0 & 0 \\ 0 & 0 & \frac{2(C+M)}{\hbar l_B} a^\dagger & \sqrt{2} v_D \\ 0 & 0 & 0 & \frac{2(C-M)}{\hbar l_B} a^\dagger \end{pmatrix} = \hat{v}_-^\dagger. \quad (15)$$

Notably, these velocity operators (with two independent 2×2 diagonal blocks) imply that the electric-dipole transitions are not active between pairs of LLs belonging to different Hamiltonians h_0 and h_0^* . This is different from magnetic-dipole transitions, which connect states originating in different Hamiltonians h_0 and h_0^* .

Taking the eigenstates $|\Psi_n\rangle$, *i.e.*, LLs expressed by Eqs. (7) and (9) arranged as:

$$|\Psi_n\rangle = \begin{pmatrix} \Phi_n \\ \Phi_n^* \end{pmatrix}, \quad (16)$$

we may calculate the selection rules sensitive to the circular polarization of the infrared radiation:

$$\begin{aligned}\langle \Psi_{n'} | \hat{v}_+(B) | \Psi_n \rangle &= \mathcal{F}_n \delta_{n,n'-1} + \mathcal{F}_n^* \delta_{n,n'+1} \quad \text{with } n \geq 0, \\ \langle \Psi_{n'} | \hat{v}_-(B) | \Psi_n \rangle &= \mathcal{F}_n \delta_{n,n'+1} + \mathcal{F}_n^* \delta_{n,n'-1} \quad \text{with } n \geq 1,\end{aligned}\tag{17}$$

where $\mathcal{F}_n = \mathcal{F}_n(A_0, \Delta, M, C, B)$ and $\mathcal{F}_n^* = \mathcal{F}_n^*(A_0, \Delta, M, C, B)$ are amplitudes belonging to transitions within the h_0 and h_0^* Hamiltonians, respectively. Importantly, we get the same selection rules for electric-dipole transitions between LLs belonging to the h_0 and h_0^* Hamiltonians, $n \rightarrow n \pm 1$. Nevertheless, the corresponding amplitudes \mathcal{F}_n and \mathcal{F}_n^* may strongly differ. Here we should again recall that the “*” symbol refers to the given sub-Hamiltonian h_0^* and does not denote the complex conjugation ($|\mathcal{F}_n^*| \neq |\mathcal{F}_n|$). The difference in amplitudes is clearly seen in the matrix elements for interband inter-LL absorption, see Fig. 8. The interband inter-LL absorption between levels belonging to the Hamiltonians h_0 and h_0^* is dominantly active in σ^- and σ^+ polarized radiation, respectively.

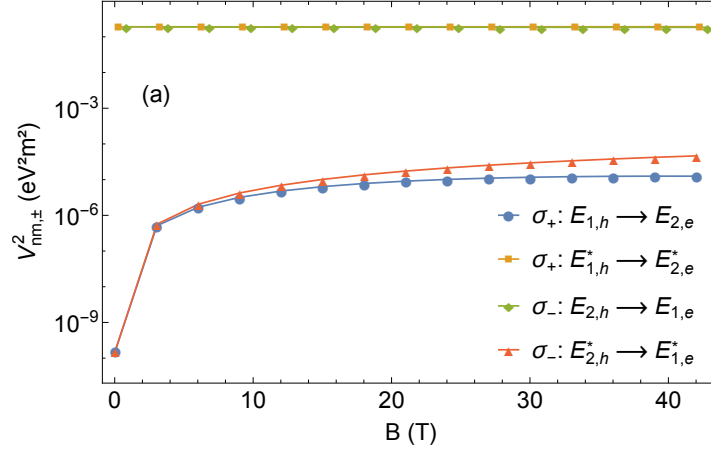


Fig. 8. Matrix elements $V_{nm,\pm}^2 = \hbar^2 |\langle \Psi_m | \hat{v}_\pm(B) | \Psi_n \rangle|^2$ for interband inter-LL transitions in Bi_2Se_3 plotted in the logarithmic scale (for $m, n = 1, 2$). For σ^- and σ^+ polarized light, interband absorption is dominated by transition between LLs originating from the h_0 and h_0^* sub-Hamiltonian, respectively.

ENERGY BAND GAP OF Bi_2Se_3

The magneto-transmission experiment, presented in this paper, provides a fairly precise estimate of the energy band gap in Bi_2Se_3 : $2\Delta = (200 \pm 4)$ meV. This result is in very good agreement with other optical studies. For instance, it matches well the value of ~ 175 and 160 meV expected for the band gap at low temperatures, as extracted from extensive reflectivity measurements on a series of bulk specimens with different electron densities in Refs. [S8] and [S9], respectively. Similarly, our results correspond very well to conclusions of recent low-temperature infrared transmission studies performed on thin layers of Bi_2Se_3 (a series of samples with thicknesses below 100 nm) prepared by molecular beam epitaxy on a (111) oriented silicon substrate [S10].

On the other hand, ARPES studies of bulk Bi_2Se_3 report gap values close to 300 meV, see, *e.g.*, Refs.[S11-13], which are significantly higher as compared to our results and other optical studies, which may invoke questions about the nature of the thin Bi_2Se_3 samples studied in these works. It is, for instance, not a priori clear whether and how the substrate properties and particular growth conditions influence the observed energy band gap and the overall band structure.

To provide another independent verification of the band gap value deduced optically, we have performed low-temperature infrared transmission measurements on thin self-standing Bi_2Se_3 layers, prepared simply by slicing bulk crystals. A typical infrared transmission spectrum is plotted in Fig. 9. This spectrum has been measured on a $10 \mu\text{m}$ -thick specimen, with the electron concentration close to 10^{18} cm^{-3} . This density has been deduced from magneto-transport measurements and it is comparable (slightly higher) with respect to the electron density in the thin film of Bi_2Se_3 studied in our magneto-transmission experiments.

The presented transmission spectrum exhibits a fairly sharp high energy cut-off at $E_g^* \approx 250$ meV. This provides us with a well-defined *upper bound* for the electronic band gap of Bi_2Se_3 , $2\Delta < E_g^*$, as schematically depicted in the

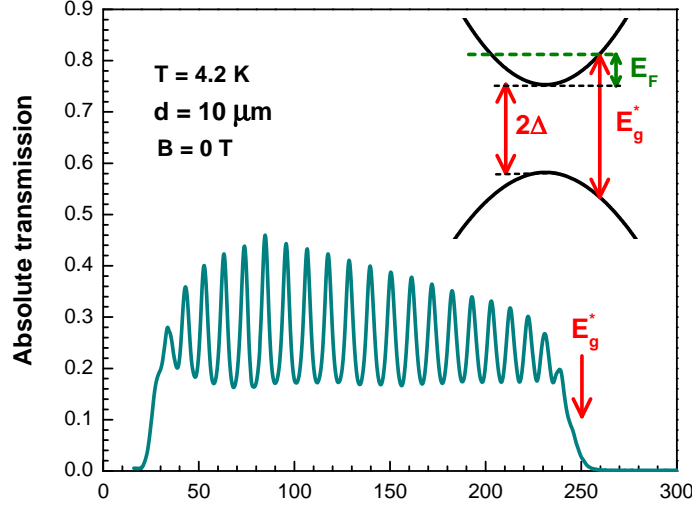


Fig. 9. Low temperature infrared transmission spectrum of a 10-micron-thick free-standing layer of Bi_2Se_3 . The inset schematically shows the relation between the high energy cut-off of the transmission spectrum and the electronic band gap: $E_g^* > 2\Delta$. The pronounced modulation of the spectrum corresponds to the Fabry-Pérot oscillations, showing rather high crystalline quality of the studied Bi_2Se_3 bulk specimen.

inset of Fig. 9. Clearly, this high-energy cut-off is significantly below the band gap of 300 meV, which is deduced from ARPES measurements. Instead, in our case, the band gap should approach $2\Delta \approx E_g^* - 2E_F \approx 200 - 210$ meV, as implied by the Burstein-Moss shift in materials with high electron-hole symmetry ($m_e \sim m_h$). The Fermi level has been estimated as $E_F = 20 - 25$ meV for the given electron density.

To conclude, the ARPES data indicate the band gap, which is significantly higher as compared to rather direct optical measurements presented in this paper as well as those performed by other groups. At present, we do not have a clear explanation for this intriguing difference, nevertheless, we speculate that ARPES is, as a matter of fact, a surface-sensitive technique. As such, the deduced band gap might be influenced by specific band-bending effects on the samples' surfaces, notably in the system with an inversed order of electronic bands. This difference clearly shows that the consensus about the size of the band gap in Bi_2Se_3 has not yet been established. This includes also on-going discussions, one versus another ARPES data, about the direct/indirect nature of the band gap in this material, see Refs. [S11-15].

ADDITIONAL EXPERIMENTAL DATA

Here we present complementary experimental data, obtained in high-field infrared magneto-transmission experiments performed on a 102 nm-thick Bi_2Se_3 layer on a $\text{InP}(111)\text{B}$ substrate. This sample was prepared using MBE technique under conditions analogous to the 290-nm-thick sample described in the main part of the paper and it is weakly n -doped with the electron density slightly below 10^{18} cm^{-3} . In spite of a lower signal-to-noise ratio obtained on this thinner sample, the observed magneto-optical response, see Figs. 10 and 11, allows us to draw the same conclusions about the electronic band structure of Bi_2Se_3 as in the case of the 290-nm-thick specimen.

The overall linear in B optical response, including intraband and interband inter-LL resonances, points towards parabolic profiles of both conduction and valence bands. The Dirac mass and the band gap (derived from the separation and low-magnetic-field extrapolation of resonances in Fig. 10, respectively) as well as the effective mass of electrons (read from CR absorption in Fig. 11) are nearly identical to values obtained from the 290-nm-thick sample: $m_D = (0.080 \pm 0.005)m_0$, $2\Delta = 190 \pm 5$ meV and $m_e = (0.14 \pm 0.1)m_0$. The parabolic profiles of electronic bands together with the condition $m_e \approx 2m_D$ thus imply also for this Bi_2Se_3 sample the specific match between spin-splitting and cyclotron energy ($E_s = 2E_c$).

In our deeper analysis, we compared (fitted) the experimentally read positions of resonances with theoretically expected transition energies calculated using full (non-linearized) expressions for LLs Eqs. (8) and (10), see the inset of Fig. 10. The best agreement was found for parameters $v_D = (0.45 \pm 0.03) \times 10^6 \text{ m.s}^{-1}$, $\Delta = (0.095 \pm 0.003) \text{ eV}$ and $M = -(22.5 \pm 1.5) \text{ eV.Å}^2$, which practically match those deduced from the 290-nm-thick sample, see the main text. The

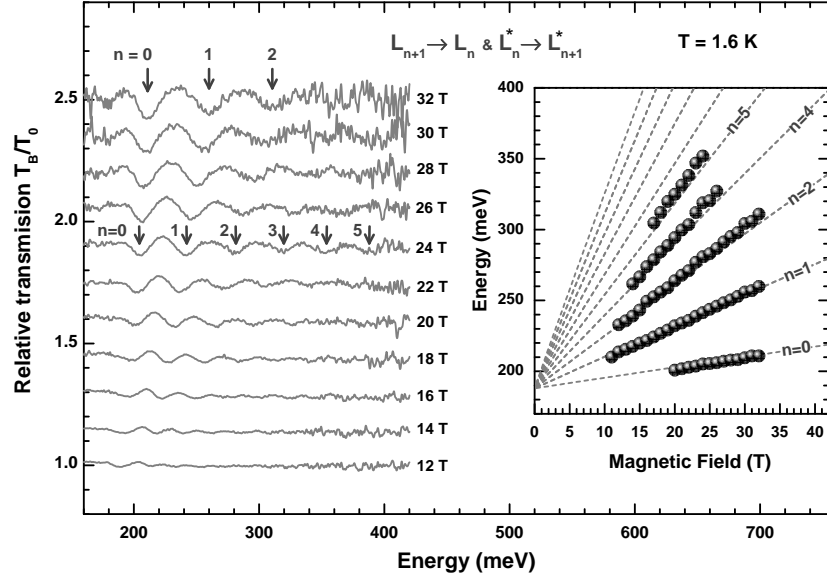


Fig. 10. Relative transmission spectra of Bi_2Se_3 in the middle infrared spectral range plotted for selected values of the magnetic field. At $B = 24$ and 32 T, individual inter-LL excitations are denoted by vertical arrows and identified by the corresponding index n . The fanchart of the observed resonances is plotted in the inset. The dashed lines represent theoretical fits described in the text (for $C \equiv 0$).

deviation from the condition $\hbar^2 v_D^2 = -4M\Delta$ for the exact parabolicity of electronic bands does not exceed a few percent for this set of parameters. This provides us with another justification for our approximation in which we describe the band structure of Bi_2Se_3 using a simplified Hamiltonian implying only two parameters: the band gap 2Δ and the velocity parameter v_D .

References:

- [S1] H. Zhang *et al.*, Nature Phys. **5**, 438 (2009).
- [S2] C.-X. Liu *et al.*, Phys. Rev. B **82**, 045122 (2010).
- [S3] M. O. Goerbig, Rev. Mod. Phys. **83**, 1193 (2011).
- [S4] L. M. Roth, B. Lax, and S. Zwerdling, Phys. Rev. **114**, 90 (1959).
- [S5] O. B. O. Ly, Electron spin resonance in topological insulators: Theoretical study, Master's thesis, Université de Strasbourg (2014).
- [S6] H. Köhler and E. Wöchner, physica status solidi (b) **67**, 665 (1975).
- [S7] B. Fauqué *et al.*, Phys. Rev. B **87**, 035133 (2013).
- [S8] H. Köhler and J. Hartmann, phys. status solidi (b) **63**, 171 (1974).
- [S9] D. Greenaway and G. Harbeke, J. Phys. Chem. Solids **26**, 1585 (1965).
- [S10] K. W. Post *et al.*, Phys. Rev. B **88**, 075121 (2013).
- [S11] Y. Xia *et al.*, Nature Phys. **5**, 398 (2009).
- [S12] Z.-H. Zhu *et al.*, Phys. Rev. Lett. **107**, 186405 (2011).
- [S13] I. A. Nechaev *et al.*, Phys. Rev. B **87**, 121111 (2013).
- [S14] O. V. Yazyev *et al.*, Phys. Rev. B **85**, 161101 (2012).
- [S15] I. Aguilera *et al.*, Phys. Rev. B **88**, 045206 (2013).
- [S16] A. M. Witowski *et al.*, Phys. Rev. B **82**, 165305 (2010).

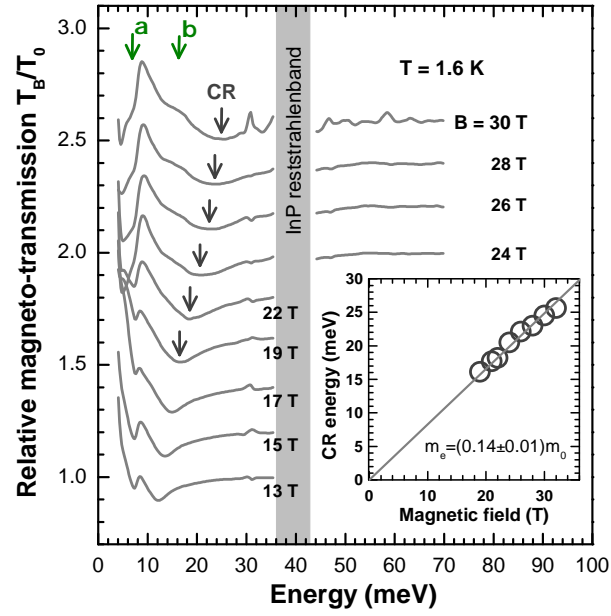


Fig. 11. Far infrared magneto-transmission spectra of the 102-nm thick Bi_2Se_3 on a InP substrate. The CR absorption is manifested as a dip in the relative magneto-transmission spectra T_B/T_0 (denoted by vertical arrows) and follows linear in B dependence, which implies the effective mass of electrons $m_e = (0.14 \pm 0.01)m_0$, see the inset. At higher magnetic fields, the response at low energies is characterized by field-induced transmission, $T_B/T_0 > 1$, which is due to suppressed zero-field Drude-type absorption, see Ref. [16] for analogous behavior in highly doped graphene. At low energies, a pronounced effect of interaction between CR and α and β phonon modes are also observed (cf. Fig. 1 in the main part of the paper).